
GAIT-BASED AGE GROUP CLASSIFICATION WITH ADAPTIVE GRAPH NEURAL NETWORK

Timilehin B. Aderinola¹; Tee Connie^{1*}; Thian Song Ong¹;
Andrew Beng Jin Teoh²; Michael Kah Ong Goh¹

¹Faculty of Information Science and Technology,
Multimedia University, Malacca, Malaysia

²School of Electrical and Electronic Engineering, College of Engineering,
Yonsei University, Seoul, South Korea

*Corresponding author: tee.connie@mmu.edu.my (Tee Connie)

ABSTRACT

Deep learning techniques have recently been utilized for model-free age-associated gait feature extraction. However, acquiring model-free gait demands accurate pre-processing such as background subtraction, which is non-trivial in unconstrained environments. On the other hand, model-based gait can be obtained without background subtraction and is less affected by covariates. For model-based gait-based age group classification problems, present works rely solely on handcrafted features, where feature extraction is tedious and requires domain expertise. This paper proposes a deep learning approach to extract age-associated features from model-based gait for age group classification. Specifically, we first develop an unconstrained gait dataset called Multimedia University Gait Age and Gender dataset (MMU GAG). Next, the body joint coordinates are determined via pose estimation algorithms and represented as compact gait graphs via a novel part aggregation scheme. Then, a Part-AdaptIve Residual Graph Convolutional Neural Network (PairGCN) is designed for age-associated feature learning. Experiments suggest that PairGCN features are far more informative than handcrafted features, yielding up to 99% accuracy for classifying subjects as a child, adult, or senior in the MMU GAG dataset.

Keywords Age classification, Feature extraction, Graph Neural Network

1 Introduction

Although the historical origin of age measurement is uncertain, it became precise with the standardization of time and date. Humans can roughly estimate age from the physical appearance when it is impossible to obtain an individual's chronological age. However, relying on eye-balling techniques for age prediction in mission-critical applications is not feasible. This motivates research in machine-based age estimation or age group classification based on physical attributes. Application areas include but are not limited to security control, surveillance, law enforcement, and human-computer interaction [1].

The two main steps in age group classification are age-associated feature extraction and classifier design. The main challenge is extracting robust age-associated features from physical attributes such as face or gait [2]. In particular, although it is possible to obtain gait from a distance with video acquisition devices, gait features are affected by covariates such as viewpoint, apparel, walking speed, walking slope, and footwear [3]. In unconstrained environments, gait can only be acquired using model-based or model-free vision-based techniques. Model-based approaches measure body part parameters such as lengths and range of motion via skeleton representations. On the other hand, model-free approaches extract features from silhouette images obtained after background subtraction. Though more computationally expensive, the model-based approaches are more robust to external covariates such as clothing and carried objects, thanks to advanced pose estimation techniques [4].

Deep learning has been widely used for age-associated feature extraction based on model-free gait descriptors such as gait energy images [5–11]. However, acquiring model-free gait requires accurate background subtraction, which is non-trivial in unconstrained environments. On the other hand, model-based gait can be obtained without background subtraction and is less affected by covariates. However, current model-based gait approaches for age estimation and age group classification [12–21] merely utilize handcrafted features, which requires domain expertise.

Recent emerging studies on Graph Neural Networks (GNNs) generalize Deep Neural Networks (DNNs) to data that cannot be represented in Euclidean space [22]. Furthermore, with recent advances in human pose estimation techniques, it is now possible to obtain joint coordinates automatically and accurately. Hence, gait can be modeled with joint coordinates as a graph, such as joints as nodes and bones as edges. This allows representation learning on model-based gait with GNNs.

This paper proposes a dedicated Graph Convolutional Network (GCN), Part-AdaptIve Residual Graph Convolutional Neural Network (PairGCN), to extract age-associated features from model-based gait in unconstrained environments, which has not been attempted before. The PairGCN can automatically adjust its edge weights based on the dominant body parts in the input part graph. More specifically, PairGCN learns which body parts are essential in classifying subjects as a child, adult, or senior by taking advantage of our part aggregation scheme.

We also introduce the gait in the wild (GITW) as the first dataset in the Multimedia University Gait Age and Gender datasets (MMU GAG)¹. GITW is naturally diverse with respect to age, race, gender, walking surface, shoe, and dressing. We impose no restrictions based on the scene, age, gender, or ethnicity, except that we restrict the collection to video recordings of healthy individuals walking at a normal pace. Table 1 compares GITW with similar existing gait datasets collected in unconstrained environments. Accordingly, GITW contains more subjects, covers more age groups, and is more naturally diverse in terms of dressing, walking surface, gender, and recording time.

Table 1: MMU GAG Datasets in Comparison With Similar Gait Datasets

Dataset	#	Age Groups*	Scene/Time	Covariates
SOTON [23]	115	-	In, out/Day	-
CASIA-B [24]	124	<i>adult</i>	In/Day	CO, DR.
USF 1 [25]	74	<i>adult</i>	Out/Day	V, TR, SH, CO, T.
USF 2 [26]	85	<i>adult</i>	Out/Day	V, TR, SH, CO, T.
Outdoor-Gait [27]	138	-	Various/Day	CL, scene, CO.
GITW (ours)	439	<i>child, adult, senior</i>	Arbitrary	Naturally diverse.

#: Number of subjects; In: Indoor; Out: Outdoor; V: view; CO: Carried Object; DR: dressing; SH: shoe; T: time; TR: terrain/walking surface. * *child* = [1–17]; *adult* = [18–64]; *senior* = [64–] years.

Our main contributions are itemized below.

1. We study age group classification problems using model-based gait features determined by the deep learning approach, which is the first of its kind.
2. A **Part-AdaptIve Residual GCN (PairGCN)** is proposed for automatic extraction of age-associated gait features in video sequences, which can incorporate age-associated part information from model-based gait.
3. A gait age and gender dataset, Gait in the Wild (GITW) is collected, pre-processed, analyzed, and released for age group classification in unconstrained environments.

2 Related Works

2.1 Age Classification and Estimation Problem using Biometric Features

The face is the most widely used biometric modality for age estimation and age group classification and has been deployed for public use [28]. Face features are broadly classified as local or holistic. Holistic-based features are obtained from the raw pixel data of faces [2, 29–32]. Local face features are obtained from the geometry of facial landmarks like eyes, mouths, and noses [33–35]. Some approaches to age group classification also use a fusion of local and holistic face features [11]. The main limitation of using face features is that performance depends on face image quality.

¹MMU GAG will be made available at https://github.com/timiderinola/mmu_gag

Other biometric features used for human age group classification include voice [36, 37] and ear images [38, 39]. However, these modalities are limited in application as data is not easily obtained in unconstrained environments. For examples, voice signals in the wild are either missing or distorted by noise, face or ear images in the wild could be partially or fully occluded.

2.2 Age Prediction Using Gait Features

Age-associated gait features could be classified as model-free or model-based. Model-free gait features are based on subjects’ shape and appearance, and extracting them involves background subtraction and silhouette generation. The most common model-free gait descriptor is the Gait Energy Image (GEI) [40]. Since GEIs are represented as grayscale images, deep learning has been widely leveraged to extract age-associated features from GEIs [5–7, 9]. In addition, some other works perform manual feature extraction from GEIs for age estimation or age group classification [41–43]. However, since obtaining silhouette images requires accurate background subtraction, obtaining model-free gait age features in the wild is infeasible.

Unlike model-free gait, model-based gait age features such as length of body segments, body ratios, and joint angles/range of motion can be manually extracted in the wild. [4] classified these features as biological, kinematic, or hybrid. Biological features are obtained from measuring body parts, such as limb length and head-to-body ratio. While biological features are sufficient to differentiate children from adults [17], more fine-grained age group classification requires kinematic features such as gait speed and joint angles [13–15, 21]. However, several model-based approaches to age group classification use biological and kinematic features [12, 16, 18–20]. The main limitation of these approaches is that manual feature extraction is tedious and requires domain expertise.

2.3 Gait Graphs for Person and Action Recognition

Until recently, model-based features had been suitable for shallow learning techniques only. However, with the recent advances in human pose estimation, it is now possible to obtain joint coordinates automatically and with high accuracy. Hence, pose-based gait analysis is receiving increasing attention. Certain studies, such as [44], have leveraged Deep Neural Networks (DNNs) for gait recognition on model-based gait features obtained via state-of-the-art pose estimation algorithms like AlphaPose [45]. Recent works such as [46–48] have automatically leveraged graph neural networks to learn gait and action recognition features. However, they are not transferred for age group classification problems.

3 Data Collection

3.1 Dataset Description

The gait in the wild (GITW) dataset contains video recordings of healthy individuals walking at a normal pace in unconstrained environments. It was collected from public domain online videos (See Figure 2). It contains 439 subjects with one clip per subject. Since the videos were collected online, the views and covariate conditions are unconstrained. The subjects were labeled with the apparent gender and age group – child, adult, or senior. The dataset has 155 children, 177 adults, and 107 seniors.

3.2 Data Preparation

Figure 1 shows the overall process followed in data preparation. Video pre-processing, pose estimation, and coordinate smoothing are discussed in this section, while body graph construction and body parts aggregation are discussed in Section 5.2.

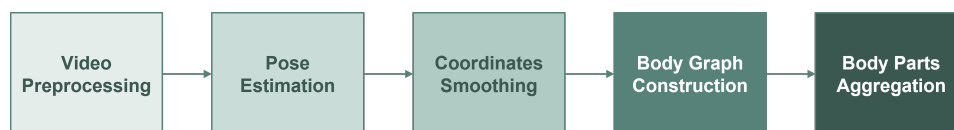


Figure 1: Data Preparation Steps



Figure 2: GITW data collection videos. Videos with pathological gait and those involving sporting activities such as running and jogging are excluded. In addition, except for seniors with walking sticks, videos of subjects with carried objects are also excluded

3.2.1 Video Preprocessing

As shown in Figure 3, GITW videos are segmented to ensure only one subject in each video. In addition, each video is segmented based on the walking direction of the participants – left, right, front, or back.

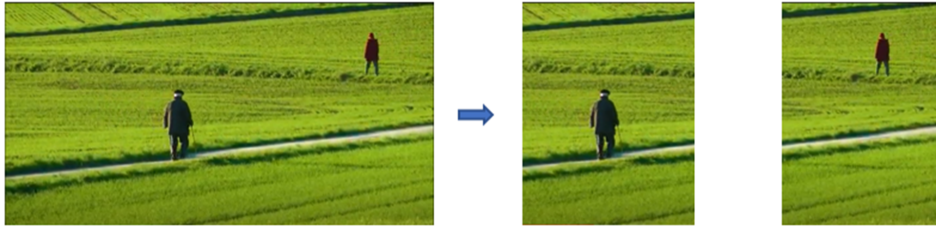


Figure 3: Video with Multiple Subjects (Left). Cropped Videos (Right). GITW videos were segmented to get the clips of interest. For example, if the subject appears only in the last 20 seconds, all the other parts of the video are discarded. Videos with multiple subjects were cropped into different videos, ensuring that each had no more than one subject.

3.2.2 Pose Estimation

Pose estimation is performed using AlphaPose [45]. For each subject with J body keypoints in a video with F frames, the pose estimation algorithm outputs a sequence of tuples $\{(x_i^t, y_i^t, c_i^t) | i = 1, \dots, J; t = 1, \dots, F\}$, where (x_i^t, y_i^t) represent the body keypoints coordinates, and $c_i^t = [0, 1]$ is the confidence score for joint i in frame t . Since videos recorded by participants are of arbitrary lengths, F is standardized to 50 frames. Hence, sequences longer than 50 frames were divided into separate frames. However, clipped sequences shorter than 25 frames were discarded as too short. For further augmentation, pose sequences were reversed, simulating the backward movement of subjects.

3.2.3 Coordinates Smoothing

The pose estimation output can be regarded as a multivariate time series, requiring some smoothing. However, smoothing with conventional filters could result in losing relevant information. Hence, we propose z-score smoothing, which replaces sudden spikes in the coordinate values with the average of the two adjacent coordinate values. Z-score smoothing works on the assumption that the motion time series data of subjects walking at a normal pace will have no sudden spikes. In the absence of sudden spikes, the data is left unchanged. After z-score smoothing, pairs of adjacent frames are averaged for dimensionality reduction, such that a sequence containing 50 frames is reduced to 25.

Let μ be the mean of $\mathbf{d} \in \mathbb{R}^F$, where \mathbf{d} is the univariate movement time series for a body keypoint across F frames. The frame-to-frame standard deviation is:

$$\sigma^2 = (1/F) \sum_{i=1}^F (d_i - \mu)^2, \sigma^2 \in \mathbb{R} \quad (1)$$

The absolute z-scores for each element in the sequence are obtained as

$$z_i = |(d_i - \mu)/\sigma|, i = 1, \dots, F; \mathbf{z} \in \mathbb{R}^F \quad (2)$$

A smoothed sequence $\mathbf{d}_s \in \mathbb{R}^F$ is then obtained according to the rule:

$$\delta_{s_i} = \begin{cases} d_i, & z_i \leq \tau, \\ (d_{i-1} + d_{i+1})/2, & \text{otherwise} \end{cases} \quad (3)$$

where τ is a threshold value defined as $\tau = (1/F) \sum_{i=1}^F z_i$. The pseudocode algorithm for z-score smoothing is given in Algorithm 1. Figure 4 illustrates the effects of z-score smoothing on a very noisy neck keypoint sequence.

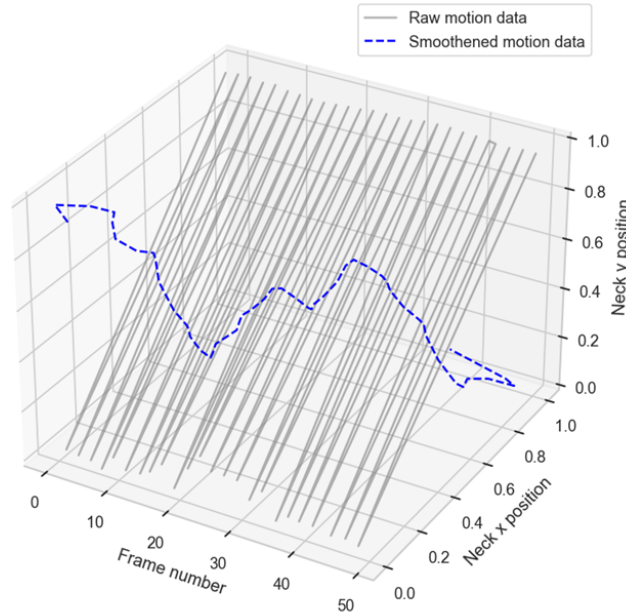


Figure 4: Coordinate Z-score Smoothing on a Noisy Sample. The sample shown in this illustration is very noisy due to false neck detections during pose estimation. These false detections result in spikes in the time series of neck motion. Z-score smoothing works on the assumption that the motion time series data of subjects walking at a normal pace will have no spikes.

Algorithm 1: Pseudocode Procedure for Z-Score Smoothing

Data: d **Result:** d_s

```
1 initialization;
2  $\mu \leftarrow MEAN(d)$ ;
3  $std \leftarrow STANDARDDEVIATION(d)$ ;
4  $z \leftarrow ABS((d - \mu)/std)$ ;
5  $threshold \leftarrow MEAN(z)$ ;
6 INITIALIZE  $i = 0$ ; list  $d_s$ ;
7 while  $i < LENGTH(d)$  do
8   if  $d_i > threshold$  then
9      $d_{s_i} \leftarrow MEAN(d_{i+1}, d_{i-1})$ 
10  else
11     $d_{s_i} \leftarrow d_i$ ;
12  end
13  INCREMENT  $i$ ;
14 end
15 RETURN  $d_s$ ;
```

4 Handcrafted Gender and Age-associated Features Extraction

In this section, we extract handcrafted gender and age-associated gait features from the GITW dataset for analysis and comparison with automatically extracted features. Let $u = \{x_i^t, y_i^t\}$ and $v = \{x_{i+1}^t, y_{i+1}^t\}$ be the coordinates of two adjacent keypoints in frame t , the Euclidean distance, D_E between u and v is given by:

$$D_E(u, v) = [(x_i^t - x_{i+1}^t)^2 + (y_i^t - y_{i+1}^t)^2]^{1/2} \quad (4)$$

Hence, as shown in Table 2, subjects' head-to-body ratio, lower limb length, hand-to-ground ratio, step length, cadence (steps per minute), and gait speed (cycles per minute) are obtained from the keypoint coordinates obtained via pose estimation. As illustrated in Figure 5, The number of steps s taken by the subject in the video is estimated by counting the peaks of the step length. The statistics of handcrafted features obtained from GITW are summarized in Table 3, and boxplots are given in Figure 6.

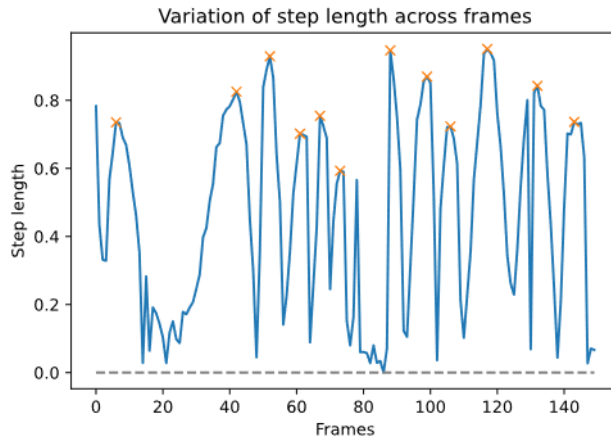


Figure 5: Obtaining step count from step length signal. The auto-detected peaks represent the heel strikes of the subjects, and the number of peaks gives the total number of steps s taken in the video.

Table 2: Definition of Features Extracted from Body Keypoints

Feature (length)	Description
$head$ (head length)	$D_E(head, neck)$
$hand$ (Upper limb length)	$D_E(shoulder, elbow) + D_E(elbow, wrist)$
$body_u$ (Upper body length)	$D_E(neck, hip)$
leg (Lower limb length)	$D_E(hip, knee) + D_E(knee, ankle)$
$stature$ (Total body length)	$head + body_u + leg$
$hand_g$ (Hand-to-ground)	$body_u + leg - hand$
$step$ (Step length)	$D_E(ankle_{left}, ankle_{right})$
$cadence$ (steps per minute)	s/N (see Figure 5)
$speed$ (gait cycles per second)	$step \times cadence$

Estimating age-associated features from pixel coordinates of $head$, $neck$, $shoulder$, $elbow$, $wrist$, hip , $knee$, and $ankle$. Except for the $ankle$, The side of the keypoints closest to the camera (left or right) is chosen.

Table 3: Gait Gender and Age-Associated Handcrafted Features Extracted from GITW Dataset

Feature	Female			Male		
	$child$ #=70	$adult$ #=77	$senior$ #=44	$child$ #=85	$adult$ #=100	$senior$ #=63
HB	0.20 ± 0.05	0.15 ± 0.02	0.15 ± 0.02	0.20 ± 0.04	0.14 ± 0.02	0.14 ± 0.03
HG	0.50 ± 0.06	0.5 ± 0.04	0.52 ± 0.04	0.49 ± 0.05	0.53 ± 0.03	0.53 ± 0.05
LG	0.42 ± 0.06	0.49 ± 0.04	0.46 ± 0.03	0.41 ± 0.05	0.48 ± 0.03	0.48 ± 0.03
SL	0.43 ± 0.15	0.33 ± 0.11	0.29 ± 0.09	0.44 ± 0.13	0.37 ± 0.10	0.32 ± 0.10
CD	52.59 ± 24.46	54.08 ± 24.65	47.01 ± 25.91	53.75 ± 26.13	65.24 ± 28.48	45.69 ± 28.12
GS	23.07 ± 13.02	19.14 ± 12.38	14.39 ± 11.38	24.43 ± 13.89	25.66 ± 15.02	15.76 ± 13.52

#: number of subjects; HB: Head-to-body ratio; HG: hand-to-ground distance; LG: lower limb length; SL: step length; CD: cadence (steps per minute); GS: gait speed (cycles per minute). Mean values are given \pm standard deviation.

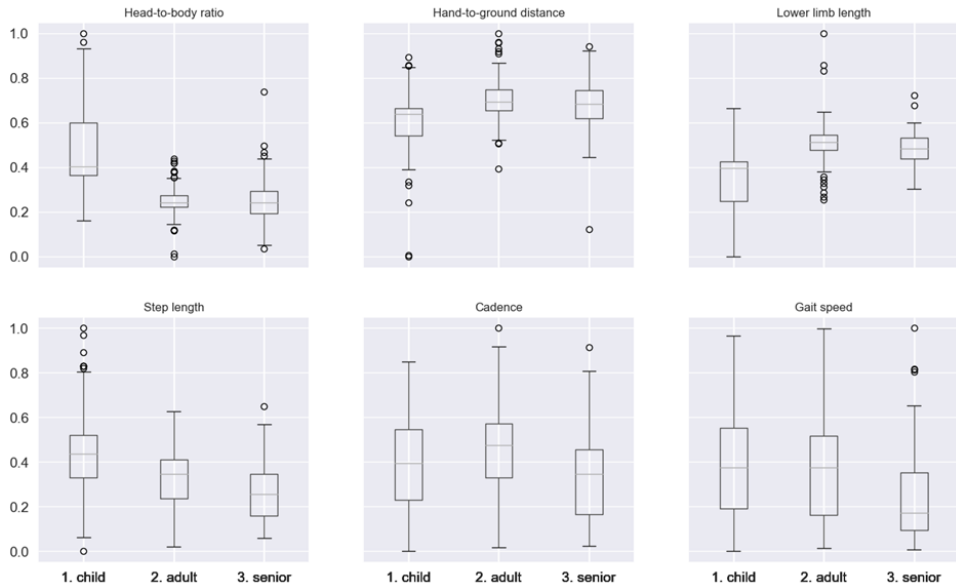


Figure 6: GITW Subjects' Average Features by Age Group

As shown in Figure 6, children in the GITW dataset are distinguishable by their greater head-to-body ratios, and they have a smaller hand-to-ground distance than the other classes. The smaller hand-to-ground distance of children follows directly from the shortness of their lower limbs compared to adults and seniors. Seniors have the slowest gait speed because they take shorter cautious steps with lower cadence.

5 Automatic Age Feature Extraction

5.1 Preliminary: Body Graph Construction

From the output of pose estimation described in Section 3.2.2, the body is modeled as a connected graph, $body = joints, bones$, where the detected joints are the nodes (the black dots in Figure 7), and the bones are edges. We represent the body graph structurally with an adjacency matrix $A_{body} \in \mathbb{R}^{J \times J}$, and feature-wise with $X_{body} \in \mathbb{R}^{J \times 3}$, where $J = |joints|$.

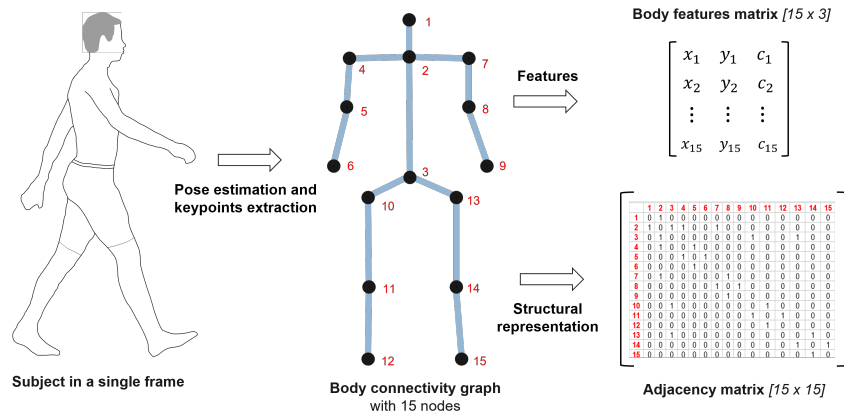


Figure 7: Body Graph Construction illustrated on a subject with 15 body keypoints

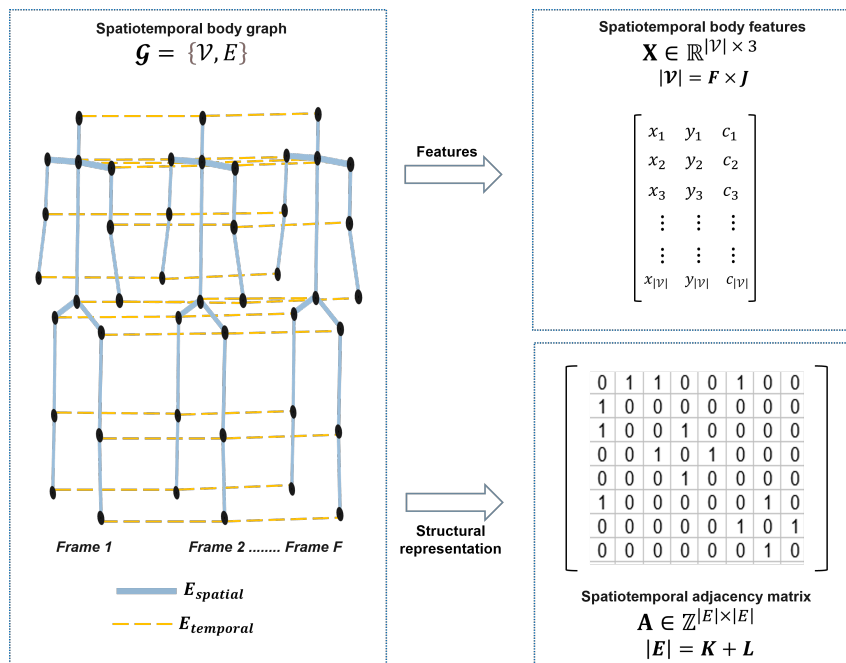


Figure 8: Spatiotemporal Body Graph Representation. Each spatiotemporal graph represents the walking motion of a single subject in a video

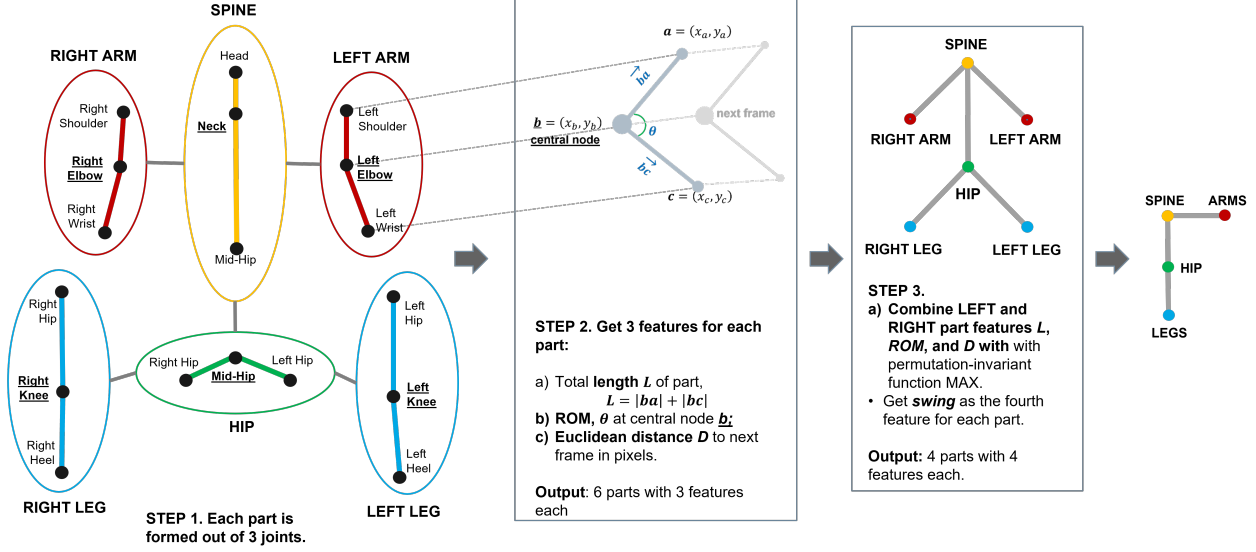


Figure 9: The Three Steps of Body Parts Aggregation. Each part consists of three nodes in the body graph aggregated to form a part node. The central node in each part is underlined and shown in bold.

Hence, we represent the walking sequence of each subject across F frames as a spatiotemporal graph $G = V, E$. $V = v_{i,j} | i = 1, \dots, F; j = 1, \dots, J$ is the set of all keypoints detected across all video frames for a subject, while $E = \{E_{spatial}, E_{temporal}\}$.

Suppose $K = |E_{spatial}|$ is the total number of bones detected across N frames, and $L = |E_{temporal}|$. Since each pair of adjacent frames has J temporal connections – one for each joint, hence $L = J(F - 2)$ and the total number of edges, $|E| = K + L$. Each body graph has a node feature matrix $X \in \mathbb{R}^{|V| \times 3}$, where $|V|$ is the number of nodes across all video frames. Structurally, the body graphs are represented by a square adjacency matrix $A \in \mathbb{Z}^{|E| \times |E|}$ that captures both spatial and local connections of body keypoint coordinates. The spatiotemporal body graph is illustrated in Figure 8.

5.2 Body Parts Aggregation

Human motion is not regarded as a movement of joint collections but as an interdependent movement of body parts, which we call aggregation of joints. For instance, with reference to Table 2, the *spine* is an essential determinant of upper body posture, consisting of the head, neck, and central hip. The *arms*, consisting of the shoulder, elbow, and wrist, are vital to balance in walking, and the arm’s motion can discriminate subjects as a child, adult, or senior (Figure 6). The body’s center of mass is at the *hip*, which comprises the left, central, and right hips. The *legs* are arguably the most critical parts of locomotion. Besides being the center of pressure, dynamic features such as gait speed, step length, and cadence are determined by leg movement, and these are crucial in more fine-grained classification. Therefore, we propose a part aggregation scheme that groups the body graph into four parts: *spine*, *arm*, *hip*, and *leg*, each made up of three joints.

As illustrated in Figure 9, each part in the part graph is associated with four features based on the raw coordinates aggregation: (a) range of motion (ROM) θ at the central node, (b) total length L of the part, (c) swing S , the distance between the left and right sides, and (d) distance D , measured as the distance in pixels covered per frame. Suppose b is the central node with a and c as its adjacent nodes. From \vec{ba} and \vec{bc} , θ and L are obtained as:

$$L = |\vec{ba}| + |\vec{bc}| \quad (5)$$

$$\theta = \cos^{-1}((\vec{ba} \cdot \vec{bc}) / |\vec{ba}| |\vec{bc}|) \quad (6)$$

Suppose that in frame i , the central node b_i for a part is at coordinate (x_{b_i}, y_{b_i}) in the 2D plane, D is obtained as the Euclidean distance between b_i and b_{i+1} :

$$D(b_i, b_{i+1}) = [(x_{b_i} - x_{b_{i+1}})^2 + (y_{b_i} - y_{b_{i+1}})^2]^{1/2} \quad (7)$$

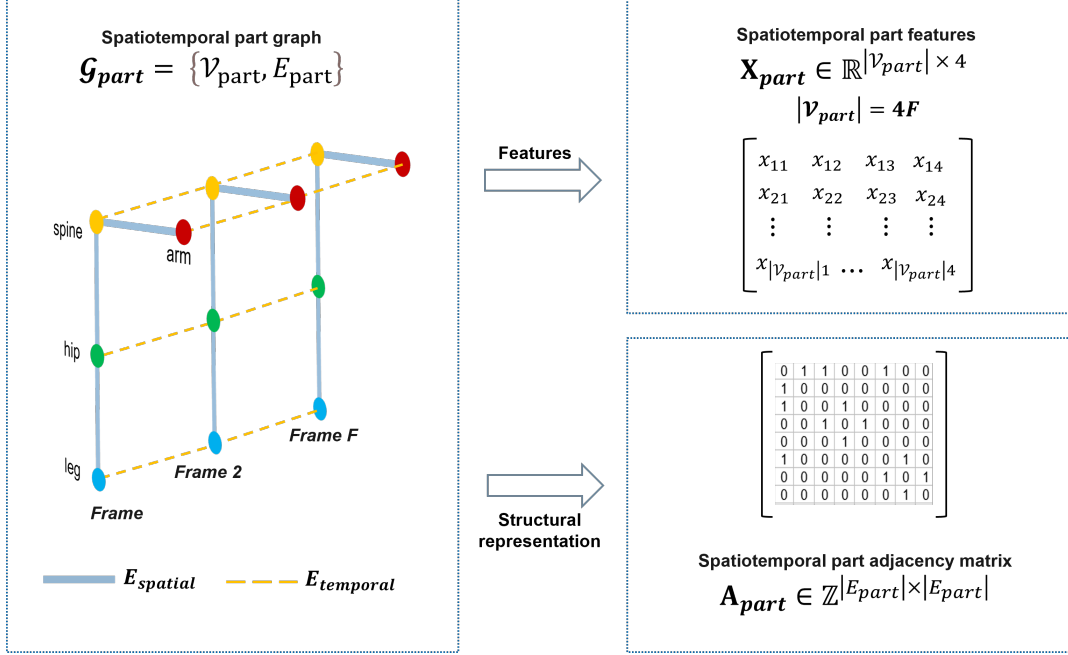


Figure 10: Spatiotemporal Parts Graph Representation

Each part has two extremes: *head* and *mid-hip* for the *spine*; *left* and *right* each for the *arm*, *leg*, and *hip*. Let p_i and q_i be the extremes for an arbitrary part in frame i . The swing S_i for each frame part is defined as:

$$S_i(p_i, q_i) = [(x_{p_i} - x_{q_i})^2 + (y_{p_i} - y_{q_i})^2]^{1/2} \quad (8)$$

Hence, the part graph is defined as a spatiotemporal graph $G_{part} = \{V_{part}, E_{part}\}$, as described in Figure 10. Each part graph has a node feature matrix $X_{part} \in \mathbb{R}^{|V_{part}| \times 4}$, where $|V_{part}| = 4F$ represents the part nodes across all video frames, each with four features described above. The E_{part} is the set of all spatial edges and temporal edges. Hence, with three spatial edges per frame and four part nodes, $|E_{part}| = 3 + 4(F - 2)$. Structurally, the part graphs are represented by a square adjacency matrix $A_{part} \in \mathbb{Z}^{|E_{part}| \times |E_{part}|}$.

5.3 Part-Adaptive Residual Graph Convolutional Neural Network

5.3.1 Preliminary

This section presents the Part-Adaptive Residual Graph Convolutional Neural Network (PairGCN) with adaptive edge weights. PairGCN takes part graphs (or body graphs) as input and learns discriminative features for children, adults, and seniors. PairGCN uses gait features only and includes an enhancement that learns edge weights for the part graph adjacency matrix in the first layer. The proposed PairGCN is based on Morris *et al.*'s GCN operator [49], given as:

$$x_i^{l+1} = \theta_1 x_i^l + \theta_2 \sum_{j \in \mathcal{N}(i)} w_{j,i} \cdot x_j^l \quad (9)$$

where, x_i^l denotes the embedding of node i (target node) in layer l ; $\mathcal{N}(i)$ is the set of neighbors of node i ; x_j^l denotes the embedding of node j (source node) in layer l ; θ_1 and θ_2 are learnable parameters; and $w_{j,i}$ is the edge weight from source node j to target node i .

In conventional GCN, $w_{j,i}$ is often set to a constant value for all edges. This often suffices in domains where the main discriminative features of the graph are the node features and graph structure. Examples include action recognition and gait recognition [38, 46, 48]. Although extracting age-associated features from a body skeleton graph also requires the body structure and joint positions represented as node features, the connectivity of the human body contains no age-associated information. The weights associated with bones and body parts and other dynamic information such as range of motion and speed must also be adequately modeled to extract age-associated features.

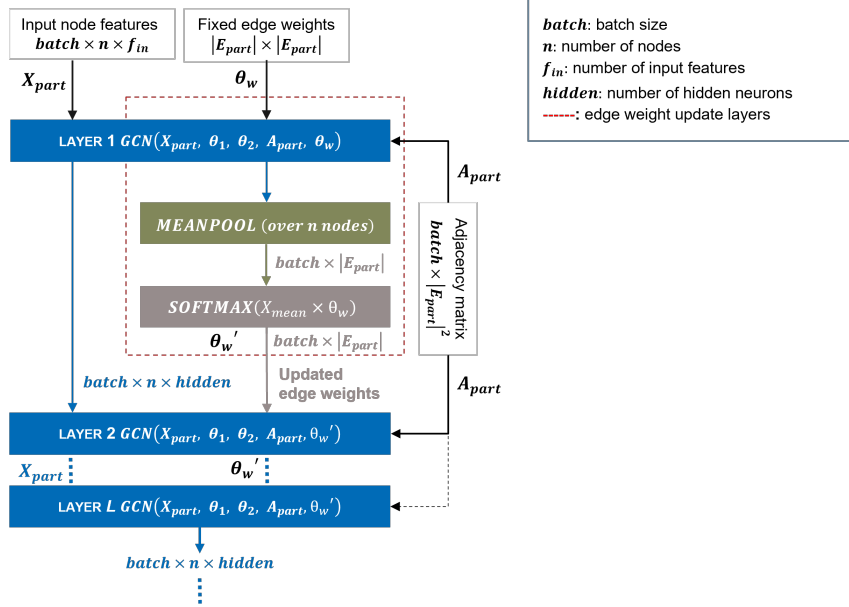


Figure 11: Updating Edge Weights (Red Dashes) in PairGCN

Therefore, the proposed PairGCN is modified from the GCN operator in Eq. 9 by introducing an adaptive edge weight $\theta_w \in \mathbb{R}^{|E_{part}|}$, such that

$$x_i^{l+1} = \theta_1 x_i^l + \theta_2 \sum_{j \in \mathcal{N}(i)} \theta_{w_{j,i}} \cdot x_j^l \quad (10)$$

How PairGCN captures age-associated features based on body parts is discussed in Section 6.1.

5.3.2 Part-adaptive GCN

As illustrated in Figure 11, the first layer of PairGCN performs the essential GCN operation according to Eq. 9. For the first layer, it makes use of a constant θ_w , initialized as 1 for each edge, and node embeddings are obtained for each graph as an aggregation of node features and their 1-hop neighborhood. Then, after the first layer, θ_w is updated based on the node embeddings obtained in the first layer as

$$\theta_w' = MEANPOOL(GCN(x^l))\theta_w \quad (11)$$

where $MEANPOOL(\cdot)$ denotes the graph-wise mean of the first layer node embeddings, $GCN(\cdot)$ refers to the forward pass performed by GCN and x^l is the node embedding in layer l , $l = 1, \dots, L$. Since edges are formed with 1-hop neighbors, edge weights θ_w are updated based on first layer node embeddings. Subsequent layers then make use of the updated edge weight in obtaining node embeddings by operating:

$$x_i^{l+1} = \theta_1 x_i^l + \theta_2 \sum_{j \in \mathcal{N}(i)} \theta'_{w_{j,i}} \cdot x_j^l \quad (12)$$

The overall architecture of PairGCN with N residual blocks is given in Figure 12. With the aid of an added fully connected layer, PairGCN is trained with the guidance of age group labels.

5.3.3 Loss Function

Data preparation steps such as augmentation and segmentation based on view introduce class imbalance in the training dataset. In PairGCN, two approaches are used to solve the class imbalance problem. Firstly, weighted random subsampling is used, such that underrepresented classes are oversampled in each training batch. Secondly, PairGCN uses a class-balanced cross-entropy loss that weights the total loss based on each class's adequate number of samples.

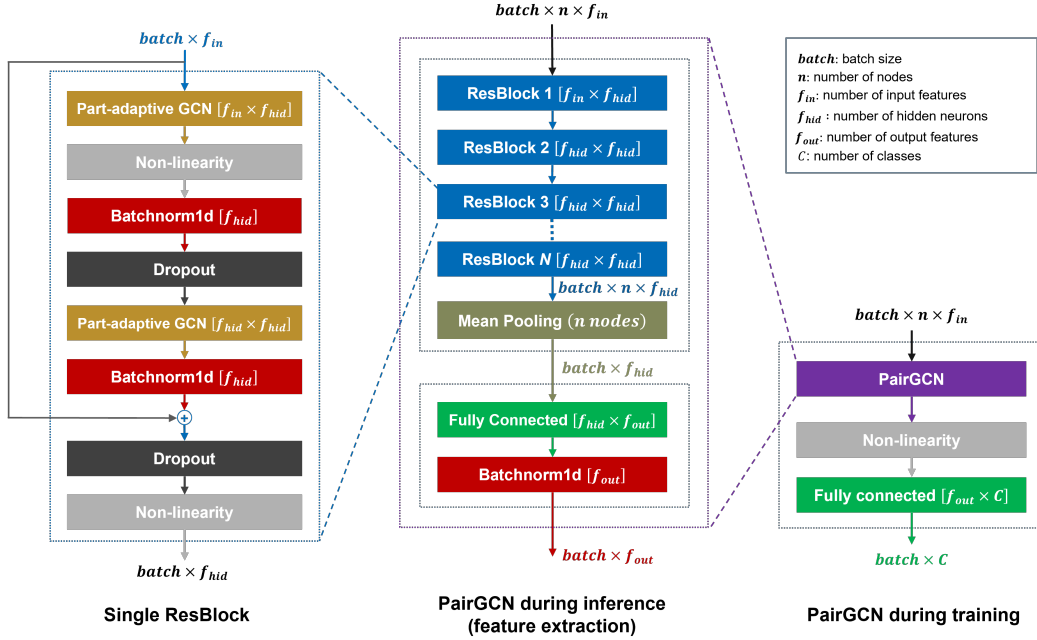


Figure 12: PairGCN Pipeline During Training and Inference

To get the weighted losses, class weights are obtained based on the effective number of samples [50] per class which is given as

$$E_c = (1 - \beta^c)/(1 - \beta) \quad (13)$$

where c = total number of samples of a class; $\beta = (N - 1)/N$; N = total number of samples. Then, the class-balanced loss L_{cb} is defined as:

$$L_{cb}(p, y) = 1/E_{c_y}(L(p, y)) \quad (14)$$

where y is the class label and p is the softmax probability. For this use case, $L(p, y)$ is the cross-entropy loss function for C classes given as:

$$L_{cb}(p, y) = (1 - \beta)/(1 - \beta^{c_y}) \sum_{i=1}^C y_i \log p_i \quad (15)$$

5.3.4 Inference

During inference, PairGCN is used as a feature extractor for unlabeled body or part graphs as input, for which it outputs a feature vector that describes the age-associated gait features in the graph. Due to age's ordinal and hierarchical nature, features obtained from PairGCN are best suited for hierarchical age group classification with tree-based classifiers such as Random Forest. However, any classifier could be fitted on the gait embedding obtained from PairGCN and used for final classification.

6 Experiments and Results

In this paper, GITW is used to evaluate the proposed method since it contains samples for *child*, *adult*, and *senior* classes. The dataset is divided into two main views with respect to the camera, namely, the front view ($0^\circ - 45^\circ$) and the side view ($45^\circ - 90^\circ$). During the training phase, each network is trained with the guidance of the age groups. In the inference stage, the trained model is used as a feature extractor to obtain the gait age signatures. For each subject, the model outputs a feature vector $f_{out} \in \mathbb{R}^{64}$, which is used as the gait age signature for age group classification.

A Random Forest classifier with 150 trees is used for age group classification. In addition to classification accuracy, the class F1 Scores are used as evaluation metrics. All experiments were conducted using three residual blocks, a learning rate of 0.001, a batch size of 64, and run for 200 epochs. The GITW dataset was divided into the train,

Table 4: List of Variables and Hyperparameters Used in Experiments

Variable/Description		Values		
		BaselineGCN	SequenceGCN	PairGCN
$batch$	Batch size	64	64	64
C	Number of classes	3	3	3
F	Total number of frames	50	50	50
f_{in}	Number of input features	3	3	4
f_{hid}	Number of hidden neurons	64	64	64
f_{out}	Number of output features	64	64	64
n	Number of nodes in input graph	15	15	4
$ E $	Spatiotemporal body graph edges	1420	N/A	N/A
$ E_b $	Bones/edges in a single frame	N/A	14	N/A
$ E_{part} $	Spatiotemporal part graph edges	N/A	N/A	342
$ E_{body} $	Sequence body graph edges	N/A	700	N/A
N	Number of residual blocks	N/A	N/A	3
	Learning rate	0.001	0.001	0.001
	Training epochs	200	200	200
	Non-linearity	<i>LeakyReLU(negative_slope = 0.01)</i>		

Table 5: Experiment Setup for the GITW dataset

View	Total Samples	After Augmentation	Train	Val	Test
$(0^\circ - 45^\circ)$	96	984	552	186	246
$(45^\circ - 90^\circ)$	224	1698	958	316	424

validation, and test sets. The train set was 75% of the dataset, and the validation set was 25% of the train set (Tables 4 and 5).

Table 6 shows that the side view of gait generally offers more age-associated features, especially for children. In comparison, the front view of gait offers more age-associated features for adults and seniors, as shown by the higher F1-score for both classes in the $(45^\circ - 90^\circ)$ view. For all views, using Random Forest gives better results.

Table 6: Summary of PairGCN Results on GITW Dataset

View	Classifier	F1 Scores			Accuracy
		<i>child</i>	<i>adult</i>	<i>senior</i>	
$(0^\circ - 45^\circ)$	PairGCN FC layer	0.95	0.83	0.88	88%
	Random Forest	0.95	0.96	0.97	96%
$(45^\circ - 90^\circ)$	PairGCN FC layer	0.95	0.90	0.82	90%
	Random Forest	0.99	0.99	0.99	99%

FC layer: fully connected layer.

6.1 An Analysis of Adaptive Weight Distributions and Body Parts

The spatiotemporal part graph obtained via parts aggregation (Figure 9) consists of spatial edges $E_{spatial}$ and temporal edges $E_{temporal}$. The spatial edges are SPINE-ARM, SPINE-HIP, and HIP-LEG, while the temporal edges are SPINE-SPINE, ARM-ARM, HIP-HIP, and LEG-LEG. Figure 15 illustrates PairGCN edge weights θ'_w for each sample. For each edge in the part graph, the edge formed by part j and i is weighted as $\theta'_{w_{j,i}} \in [0, 1]$. These weights are averaged for each age group (Figure 13).

The SPINE-ARM and ARM-ARM connections are important in discriminating between children and other age groups. This is as expected since children are easily distinguishable by their arm swings. However, the arm movement of seniors is often more cautious since they're prone to falls. On the other hand, SPINE-HIP and HIP-LEG connections

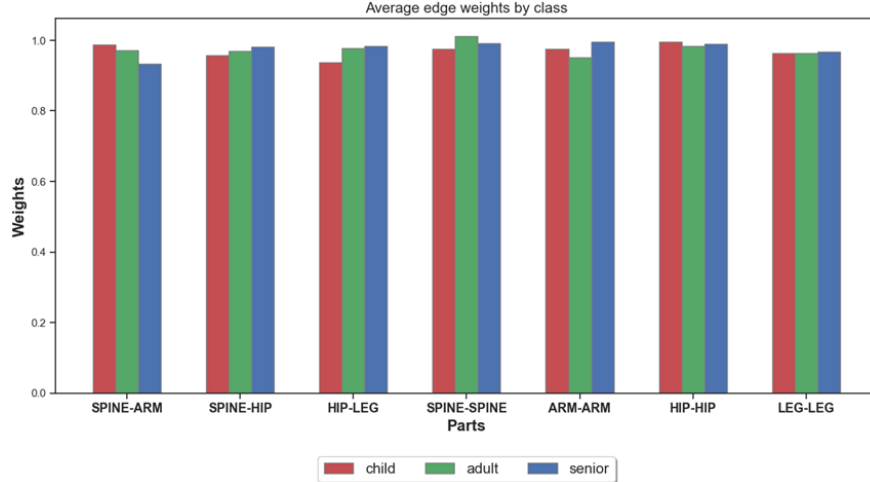


Figure 13: PairGCN Average Edge Weights by Class

are assigned greater weights in distinguishing seniors. This follows since seniors have a greater range of motion at the hips and lower extremity joints. The equally weighted LEG-LEG connection indicates the universal importance of dynamic features such as gait speed, step length, and cadence, which depend on the temporal movement of the lower limbs.

6.2 Ablation Studies

This section demonstrates the ablation studies on the performance of PairGCN architecture, adaptive edge weights, body parts aggregation, coordinate smoothing, and view regarding age classification accuracy and F1 scores on the GITW dataset.

A. PairGCN vs. Baseline GCN Architecture

GCN architectures are often highly task-specific. For comparison, a baseline GCN architecture (Figure 14) is constructed according to the basic architecture proposed by [51]. As shown in Table 7, PairGCN achieves the highest overall accuracy on the GITW dataset in the $45^\circ - 90^\circ$ view. As expected, the Baseline GCN and PairGCN both learn more age-associated features in the side view of gait. This is expected since most age-associated features such as arm swing, posture, step length, stride length, upper and lower limb range of motion, and minimum toe clearance are found in the side view of gait. The front view of gait presents mostly static features, while the side view is rich with both static and dynamic spatiotemporal gait features.

Table 7: Effects of Different Settings on Accuracy

	Arch.	Settings			View	Accuracy
		Adaptive Weights	Aggr. Features	Smoothing		
1.	BaselineGCN	×	×	✓	$45^\circ - 90^\circ$	0.94
2.		×	✓	✓	$45^\circ - 90^\circ$	0.96
3.		×	✓	✓	$0^\circ - 45^\circ$	0.97
4.	PairGCN	✓	✓	✓	$0^\circ - 45^\circ$	0.96
5.		×	✓	✓	$45^\circ - 90^\circ$	0.98
6.		✓	×	✓	$45^\circ - 90^\circ$	0.98
7.		✓	✓	✓	$45^\circ - 90^\circ$	0.99

Table 8: Effects of Different Settings on F1 Scores

	Arch.	Settings			F1 Scores		
		Adaptive Weights	Aggr. Features	Smoothing	<i>child</i>	<i>adult</i>	<i>senior</i>
1.	BaselineGCN	×	×	✓	0.98	0.94	0.89
2.		×	✓	✓	0.98	0.96	0.95
3.	PairGCN	×	✓	✓	0.99	0.98	0.97
4.		✓	×	✓	0.99	0.98	0.96
5.		✓	✓	×	1.00	0.99	0.97
6.		✓	✓	✓	0.99	0.99	0.99

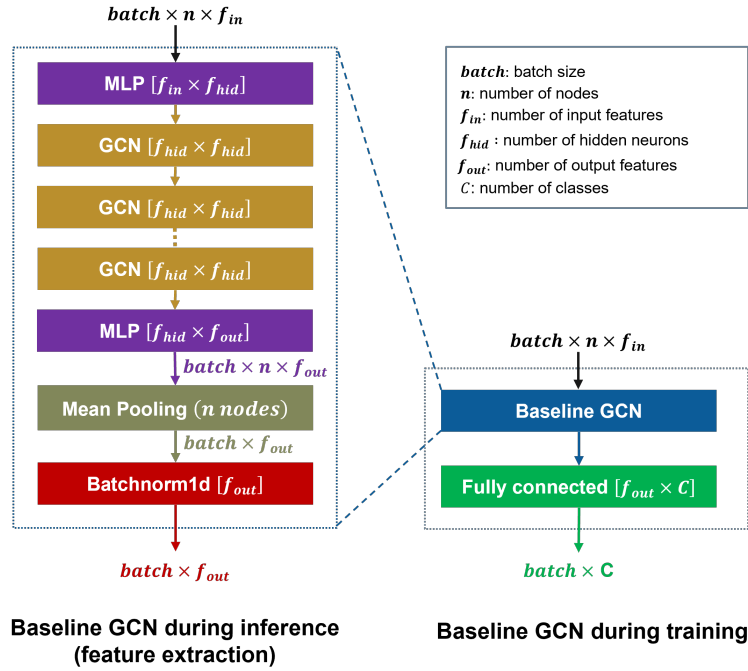


Figure 14: Baseline GCN Architecture

B. Adaptive Edge Weighting

The performance of PairGCN with adaptive edge weights is compared to its performance with constant edge weights on the $45^\circ - 90^\circ$ view of the GITW dataset. PairGCN without adaptive edge weights shows better F1 Scores for children than the older age groups in Table 8. This suggests that it becomes increasingly difficult to discriminate against older age groups without adaptive edge weighting.

C. Part Aggregation vs. Raw Coordinates

The performance of part aggregation is compared to raw coordinates for age group classification, using the Baseline GCN and PairGCN on the $45^\circ - 90^\circ$ view of the GITW dataset. The two methods are compared in model performance (Tables 7 and 8). Part aggregation improves the performance of both architectures.

D. Coordinate Smoothing

As shown in Table 8, the F1 scores suggest that without smoothing, PairGCN finds it increasingly difficult to learn features associated with age groups as the age increases. While it is straightforward to learn features associated with children (such as their body size) even with noisy coordinates, the features associated with adults and seniors are more subtle and sensitive to noise.

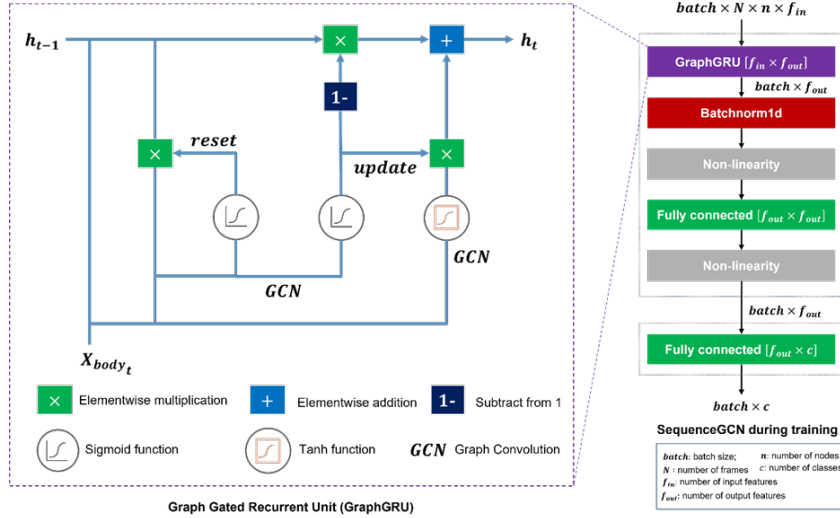


Figure 15: SequenceGCN Architecture

Table 9: SequenceGCN Results on GITW

Method	Accuracy	Class F1 Scores		
		<i>child</i>	<i>adult</i>	<i>senior</i>
Gait as a Sequence (SequenceGCN)	39%	0.29	0.53	0.10
Spatiotemporal Gait (PairGCN)	99%	0.99	0.99	0.99

6.3 The Importance of Temporal Gait Information

In sequential data and time-series analysis, recurrent neural networks (RNNs) such as Long-Short Term Memory (LSTM) [52] have achieved outstanding results in sequential classification and prediction. While it may seem more natural to model gait as a sequence and adopt RNNs, this section presents a comparative analysis between spatiotemporal and sequence-based gait for age group classification. A Sequence GCN with a Graph Gated Recurrent Unit (GraphGRU) architecture is constructed for this analysis, as illustrated in Figure 15.

Sequence gait graphs are obtained where each subject is represented by a sequence of body graphs, with one body graph for each input video frame. Each body graph consists of joints as vertices, and bones as edges, defined as $G_b = \{V_b, E_b\}$, $V_b = V_{b_i} | i = 1, \dots, J$; $E_b = E_{b_j} | j = 1, \dots, |E_{body}|$. Structurally, the body graphs are represented by an identical square adjacency matrix $A_b \in \mathbb{Z}^{|E_b| \times |E_b|}$, where $|E_b|$ is the number of bones/edges. Hence, for F frames, each subject’s gait sequence is represented as a sequence of body graphs, $G_{seq} = G_{b_1}, \dots, G_{b_F}$. SequenceGCN is trained using G_{seq} and A_b with the guidance of age group labels.

SequenceGCN (Table 9) suggests that the network cannot learn age-associated features from gait modeled as a sequence. Several reasons could be given for this observation. First, although gait is observed from the walking sequence of subjects, gait is more of a cycle than a sequence. However, sequence-based methods such as SequenceGCN will consider each frame in the context of previous frames while failing to consider the temporal connections between the frames. Hence, modeling gait as a spatiotemporal graph is more suitable for age group classification. In contrast, modeling gait as a sequence of body graphs is perhaps more suited to naturally sequence-based tasks such as human action recognition.

6.4 Comparison With Existing Methods

PairGCN is proposed to extract age-associated model-based gait features for age group classification. However, at the time of this writing, existing model-based gait techniques for age group classification make use of handcrafted features and perform classification with conventional classifiers such as Random Forest [12, 53], Support Vector Machines [13, 18, 20, 54], and K-Nearest Neighbour [14, 16].

Table 10: Comparison of Manually Extracted Features with PairGCN Features

Feature Extraction	Works	Final Classifier	Acc.	Class F1 Scores		
				<i>child</i>	<i>adult</i>	<i>senior</i>
Handcrafted	[54], [18]	SVM (linear kernel)	64%	0.78	0.67	0.14
	[13], [20]	SVM (RBF kernel)	74%	0.85	0.72	0.62
	[16]	KNN (k=26)	73%	0.82	0.73	0.54
	[14]	KNN (k=5)	80%	0.86	0.80	0.72
	[53]	RF (100 trees)	89%	0.91	0.91	0.84
	[12]	RF (150 trees)	89%	0.92	0.91	0.84
Learned	BaselineGCN [51]	RF (150 tree)	97%	0.97	0.96	0.99
	PairGCN (ours)	PairGCN FC	90%	0.94	0.90	0.82
		SVM (RBF kernel)	98%	0.99	0.97	0.97
		KNN (k=5)	96%	0.99	0.95	0.93
		RF (150 trees)	99%	0.99	0.99	0.99

The best values are shown in a **bold** font face. SVM: Support Vector Machine; RBF: Radial Basis Function; KNN: K-Nearest Neighbour; RF: Random Forest.

This section compares features extracted using PairGCN with the performance of handcrafted features, using SVM, KNN, and RF as classifiers. The best-performing settings of the classifiers are chosen for comparison. The results in Table 10 show that compared to manually extracted features, PairGCN features contain richer age-associated features. It is also observed that the accuracy can be further improved with classifiers such as SVM, KNN, or Random Forests.

6.5 Discussion

Adaptive weighting in PairGCN enables PairGCN to learn the importance of body parts. Experiments indicate that part-based features offer higher accuracy, smoother convergence, and faster runtime. In addition, the side view of gait offers more age-associated features in general, especially for children. In comparison, the front view of gait offers more age-associated features for adults and seniors.

Body coordinate features are inherently noisy due to false detections and multiple detections of joints during pose estimation. However, experiments show performance improvements with smoothing. The experiments also suggest that the age-associated features of the elderly are subtle and more sensitive to noise than children, as children can easily be detected by their smaller body sizes and larger head-to-body ratios.

Although gait is measured from the walking sequence of humans, it is more of a cycle than a sequence. Hence, experiments suggest that it is best to model gait as a large spatiotemporal graph to capture the inter-frame temporal information, which is crucial in age discrimination. The finding also corroborates this observation that several spatiotemporal gait features are measured from the inter-frame connections of joints.

7 Conclusion and Future Research

Though the Graph Neural Network architectures proposed in this research achieve high accuracy on the side view of gait, the performance degrades on view change. The viewpoint challenge is common to all gait-related tasks. Graph Neural Network architectures are also task-sensitive; the network must be tuned differently for each task. Domain adaptation has been applied in tasks like character recognition, enabling a model to perform comparably well on a dataset slightly different from the dataset it was trained on. Future research can achieve view-invariant gait-based age group classification by using domain adaptation.

PairGCN validation losses are relatively high (around 20%) due to the noisy nature of coordinates and the variability of age-associated gait features. For example, a child might have a gait like an adult and vice-versa. In addition, PairGCN is sensitive to task change and prone to overfitting on the gait graphs. Hence, features extracted using PairGCN are best used with classifiers that are more robust to the irregularities in age-associated features.

In this study, we perform age classification with a limited level of granularity. However, some contexts may require more fine-grained age prediction. Therefore, future research will focus on increasing the granularity of age classification.

Acknowledgement

This work was supported by Multimedia University IR Fund under Grant MMUI/220026.

References

- [1] Raphael Angulu, Jules R. Tapamo, and Aderemi O. Adewumi. Age estimation via face images: a survey. *EURASIP Journal on Image and Video Processing*, 2018(1):42, 2018. doi: 10.1186/s13640-018-0278-6.
- [2] Haibin Liao, Yuchen Yan, Wenhua Dai, and Ping Fan. Age estimation of face images based on CNN and divide-and-rule strategy. *Mathematical Problems in Engineering*, 2018.
- [3] T. Connie, K. O. M. Goh, and A. Beng Jin Teoh. A review for gait recognition across view. In *2015 3rd International Conference on Information and Communication Technology (ICoICT)*, pages 574–577, 2015. doi: 10.1109/ICoICT.2015.7231488.
- [4] Timilehin B. Aderinola, Tee Connie, Thian Song Ong, Wei-Chuen Yau, and Andrew Beng Jin Teoh. Learning age from gait: A survey. *IEEE Access*, 9:100352–100368, 2021. doi: 10.1109/ACCESS.2021.3095477.
- [5] Murat Berkkan. *Gender recognition and age estimation based on human gait*. PhD thesis, Başkent Üniversitesi Fen Bilimleri Enstitüsü, 2019.
- [6] M. J. Marín-Jiménez, F. M. Castro, N. Guil, F. de la Torre, and R. Medina-Carnicer. Deep multi-task learning for gait-based biometrics. In *2017 IEEE International Conference on Image Processing (ICIP)*, pages 106–110, 2017. doi: 10.1109/ICIP.2017.8296252.
- [7] Newlin Shebiah Russel and Arivazhagan Selvaraj. Gender discrimination, age group classification and carried object recognition from gait energy image using fusion of parallel convolutional neural network. *IET Image Processing*, 15(1):239–251, 2021. doi: <https://doi.org/10.1049/ipr2.12024>.
- [8] Atsuya Sakata, Yasushi Makihara, Noriko Takemura, Daigo Muramatsu, and Yasushi Yagi. Gait-based age estimation using a DenseNet. In Gustavo Carneiro and Shaodi You, editors, *Computer Vision – ACCV 2018 Workshops*, pages 55–63. Springer International Publishing, 2019. doi: 10.1007/978-3-030-21074-8_5.
- [9] Atsuya Sakata, Noriko Takemura, and Yasushi Yagi. Gait-based age estimation using multi-stage convolutional neural network. *IPSN Transactions on Computer Vision and Applications*, 11(1):4, 2019.
- [10] X. Li, Y. Makihara, C. Xu, Y. Yagi, and M. Ren. Make the bag disappear: Carrying status-invariant gait-based human age estimation using parallel generative adversarial networks. In *2019 IEEE 10th International Conference on Biometrics Theory, Applications and Systems (BTAS)*, pages 1–9, 2019. doi: 10.1109/BTAS46853.2019.9185973.
- [11] Ke Zhang, Na Liu, Xingfang Yuan, Xinyao Guo, Ce Gao, Zhenbing Zhao, and Zhanyu Ma. Fine-grained age estimation in the wild with attention LSTM networks. *arXiv:1805.10445 [cs]*, 2018.
- [12] Timilehin B. Aderinola, Tee Connie, Thian Song Ong, and Kah Ong Michael Goh. Automatic extraction of spatio-temporal gait features for age group classification. In Lalit Garg, Hemant Sharma, S. B. Goyal, and Amarpreet Singh, editors, *Proceedings of International Conference on Innovations in Information and Communication Technologies*, pages 71–78. Springer, 2021. doi: 10.1007/978-981-16-0873-5_6.
- [13] R.K. Begg, M. Palaniswami, and B. Owen. Support vector machines for automated gait classification. *IEEE Transactions on Biomedical Engineering*, 52(5):828–838, 2005. doi: 10.1109/TBME.2005.845241.
- [14] Chang Yang and Wenyong Wang. A novel age interval identification method based on gait monitoring. In *2015 4th International Conference on Computer Science and Network Technology (ICCSNT)*, volume 01, pages 266–269, 2015. doi: 10.1109/ICCSNT.2015.7490749.
- [15] James W. Davis. Visual categorization of children and adult walking styles. In *Proceedings of the Third International Conference on Audio- and Video-Based Biometric Person Authentication, AVBPA '01*, pages 295–300. Springer-Verlag, 2001.
- [16] Houman Hediye, Tarek Sayed, and Mohamed H. Zaki. Use of spatiotemporal parameters of gait for automated classification of pedestrian gender and age. *Transportation Research Record*, 2393(1):31–40, 2013. doi: 10.3141/2393-04.
- [17] Omer F. Ince, J. S. Park, J. Song, and B. W. Yoon. Child and adult classification using ratio of head and body heights in images. *International Journal of Computer and Communication Engineering*, 3(2):120–122, 2014. doi: 10.7763/IJCCE.2014.V3.304.

- [18] M. Hema and S. Pitta. Human age classification based on gait parameters using a gait energy image projection model. In *2019 3rd International Conference on Trends in Electronics and Informatics (ICOEI)*, pages 1163–1168, 2019. doi: 10.1109/ICOEI.2019.8862788.
- [19] Prachi Punyani, Rashmi Gupta, and Ashwani Kumar. Human age-estimation system based on double-level feature fusion of face and gait images. *International Journal of Image and Data Fusion*, 9(3):222–236, 2018. doi: 10.1080/19479832.2018.1423644.
- [20] Hyun Woo Yoo and Ki Youn Kwon. Method for classification of age and gender using gait recognition. *Transactions of the Korean Society of Mechanical Engineers A*, 41(11):1035–1045, 2017. doi: 10.3795/KSME-A.2017.41.11.1035.
- [21] D. Zhang, Y. Wang, and B. Bhanu. Age classification base on gait using HMM. In *2010 20th International Conference on Pattern Recognition*, pages 3834–3837, 2010. doi: 10.1109/ICPR.2010.934.
- [22] Michael M. Bronstein, Joan Bruna, Yann LeCun, Arthur Szlam, and Pierre Vandergheynst. Geometric deep learning: Going beyond euclidean data. *IEEE Signal Processing Magazine*, 34(4):18–42, 2017. doi: 10.1109/MSP.2017.2693418.
- [23] J. D. Shutler, M. G. Grant, M. S. Nixon, and J. N. Carter. On a large sequence-based human gait database. In Ahamad Lotfi and Jonathan M. Garibaldi, editors, *Applications and Science in Soft Computing*, Advances in Soft Computing, pages 339–346. Springer, 2004. doi: 10.1007/978-3-540-45240-9_46.
- [24] Shiqi Yu, Daoliang Tan, and Tieniu Tan. A framework for evaluating the effect of view angle, clothing and carrying condition on gait recognition. In *18th International Conference on Pattern Recognition (ICPR'06)*, volume 4, pages 441–444, 2006. doi: 10.1109/ICPR.2006.67.
- [25] P.J. Phillips, S. Sarkar, I. Robledo, P. Grother, and K. Bowyer. Baseline results for the challenge problem of HumanID using gait analysis. In *Proceedings of Fifth IEEE International Conference on Automatic Face Gesture Recognition*, pages 137–142, 2002. doi: 10.1109/AFGR.2002.1004145.
- [26] S. Sarkar, P.J. Phillips, Z. Liu, I.R. Vega, P. Grother, and K.W. Bowyer. The humanID gait challenge problem: data sets, performance, and analysis. *IEEE Transactions on Pattern Analysis and Machine Intelligence*, 27(2): 162–177, 2005. doi: 10.1109/TPAMI.2005.39.
- [27] Chunfeng Song, Yongzhen Huang, Yan Huang, Ning Jia, and Liang Wang. GaitNet: An end-to-end network for gait based human identification. *Pattern Recognition*, 96:106988, 2019. doi: 10.1016/j.patcog.2019.106988.
- [28] Chris Burt. Biometrics could help gaming industry with cybercrime, age verification as market evolves | biometric update, 2020.
- [29] Shixing Chen, Caojin Zhang, and Ming Dong. Deep age estimation: From classification to ranking. *IEEE Transactions on Multimedia*, 20(8):2209–2222, 2018. doi: 10.1109/TMM.2017.2786869.
- [30] Wei Shen, Yilu Guo, Yan Wang, Kai Zhao, Bo Wang, and Alan Loddon Yuille. Deep differentiable random forests for age estimation. *IEEE Transactions on Pattern Analysis and Machine Intelligence*, pages 1–1, 2019. doi: 10.1109/TPAMI.2019.2937294.
- [31] Jiu-Cheng Xie and Chi-Man Pun. Chronological age estimation under the guidance of age-related facial attributes. *IEEE Transactions on Information Forensics and Security*, 14(9):2500–2511, 2019. doi: 10.1109/TIFS.2019.2902823.
- [32] Zijiang Zhu, Hang Chen, Yi Hu, and Junshan Li. Age estimation algorithm of facial images based on multi-label sorting. *EURASIP Journal on Image and Video Processing*, 2018(1):114, 2018. doi: 10.1186/s13640-018-0353-z.
- [33] G. Guo, Guowang Mu, Y. Fu, and T. S. Huang. Human age estimation using bio-inspired features. In *2009 IEEE Conference on Computer Vision and Pattern Recognition*, pages 112–119, 2009. doi: 10.1109/CVPR.2009.5206681.
- [34] K. Chang and C. Chen. A learning framework for age rank estimation based on face images with scattering transform. *IEEE Transactions on Image Processing*, 24(3):785–798, 2015. doi: 10.1109/TIP.2014.2387379.
- [35] Young Ho Kwon and da Vitoria Lobo. Age classification from facial images. In *1994 Proceedings of IEEE Conference on Computer Vision and Pattern Recognition*, pages 762–767, 1994. doi: 10.1109/CVPR.1994.323894.
- [36] Damian Kwasny and Daria Hemmerling. Gender and age estimation methods based on speech using deep neural networks. *Sensors*, 21(14), 2021. doi: 10.3390/s21144785.

- [37] Shijing Si, Jianzong Wang, Junqing Peng, and Jing Xiao. Towards speaker age estimation with label distribution learning. In *ICASSP 2022 - 2022 IEEE International Conference on Acoustics, Speech and Signal Processing (ICASSP)*, pages 4618–4622, 2022. doi: 10.1109/ICASSP43922.2022.9746378.
- [38] Dogucan Yaman, Fevziye Irem Eyiokur, Nurdan Sezgin, and Hazim Kemal Ekenel. Age and gender classification from ear images. In *2018 International Workshop on Biometrics and Forensics (IWBF)*, pages 1–7, 2018. doi: 10.1109/IWBF.2018.8401568.
- [39] Dogucan Yaman, Fevziye Irem Eyiokur, and Hazim Kemal Ekenel. Multimodal age and gender classification using ear and profile face images. In *Proceedings of the IEEE/CVF Conference on Computer Vision and Pattern Recognition Workshops*, pages 0–0, 2019.
- [40] Ju Han and Bir Bhanu. Individual recognition using gait energy image. *IEEE Transactions on Pattern Analysis and Machine Intelligence*, 28(2):316–322, 2006. doi: 10.1109/TPAMI.2006.38.
- [41] Y. Makihara, M. Okumura, H. Iwama, and Y. Yagi. Gait-based age estimation using a whole-generation gait database. In *2011 International Joint Conference on Biometrics (IJCB)*, pages 1–6, 2011. doi: 10.1109/IJCB.2011.6117531.
- [42] N. Mansouri, M. Aouled Issa, and Y. Ben Jemaa. Gait features fusion for efficient automatic age classification. *IET Computer Vision*, 12(1):69–75, 2018. doi: 10.1049/iet-cvi.2017.0055.
- [43] M. Nabila, A. I. Mohammed, and B. J. Yousra. Gait-based human age classification using a silhouette model. *IET Biometrics*, 7(2):116–124, 2018. doi: 10.1049/iet-bmt.2016.0176.
- [44] Rijun Liao, Chunshui Cao, Edel B. Garcia, Shiqi Yu, and Yongzhen Huang. Pose-based temporal-spatial network (PTSN) for gait recognition with carrying and clothing variations. In Jie Zhou, Yunhong Wang, Zhenan Sun, Yong Xu, Linlin Shen, Jianjiang Feng, Shiguang Shan, Yu Qiao, Zhenhua Guo, and Shiqi Yu, editors, *Biometric Recognition*, pages 474–483. Springer International Publishing, 2017. doi: 10.1007/978-3-319-69923-3_51.
- [45] Hao-Shu Fang, Shuqin Xie, Yu-Wing Tai, and Cewu Lu. RMPE: Regional multi-person pose estimation. *arXiv:1612.00137 [cs]*, 2018.
- [46] Na Li, Xinbo Zhao, and Chong Ma. JointsGait:a model-based gait recognition method based on gait graph convolutional networks and joints relationship pyramid mapping. *arXiv:2005.08625 [cs, eess]*, 2020.
- [47] Rijun Liao, Shiqi Yu, Weizhi An, and Yongzhen Huang. A model-based gait recognition method with body pose and human prior knowledge. *Pattern Recognition*, 98:107069, 2020. doi: 10.1016/j.patcog.2019.107069.
- [48] Torben Teepe, Ali Khan, Johannes Gilg, Fabian Herzog, Stefan Hormann, and Gerhard Rigoll. Gaitgraph: Graph convolutional network for skeleton-based gait recognition. *2021 IEEE International Conference on Image Processing (ICIP)*, Sep 2021. doi: 10.1109/icip42928.2021.9506717.
- [49] Christopher Morris, Martin Ritzert, Matthias Fey, William L. Hamilton, Jan Eric Lenssen, Gaurav Rattan, and Martin Grohe. Weisfeiler and leman go neural: Higher-order graph neural networks. *Proceedings of the AAAI Conference on Artificial Intelligence*, 33:4602–4609, Jul 2019. doi: 10.1609/aaai.v33i01.33014602.
- [50] Yin Cui, Menglin Jia, Tsung-Yi Lin, Yang Song, and Serge Belongie. Class-balanced loss based on effective number of samples. *2019 IEEE/CVF Conference on Computer Vision and Pattern Recognition (CVPR)*, Jun 2019. doi: 10.1109/cvpr.2019.00949.
- [51] Jiaxuan You, Rex Ying, and Jure Leskovec. Design space for graph neural networks. In *Proceedings of the 34th International Conference on Neural Information Processing Systems, NIPS’20*. Curran Associates Inc., 2020. ISBN 9781713829546.
- [52] Sepp Hochreiter and Jürgen Schmidhuber. Long short-term memory. *Neural computation*, 9(8):1735–1780, 1997.
- [53] M. Hema, K. Babulu, and N. Balaji. Gait based human age classification using random forest classifier. *i-manager’s Journal on Pattern Recognition*, 6(2):1–7, 2019.
- [54] B. K. Y. Chuen, T. Connie, O. T. Song, and M. Goh. A preliminary study of gait-based age estimation techniques. In *2015 Asia-Pacific Signal and Information Processing Association Annual Summit and Conference (APSIPA)*, pages 800–806, 2015. doi: 10.1109/APSIPA.2015.7415382.